Geophysical Journal International

*Geophys. J. Int.* (2018) **215,** 37–48
Advance Access publication 2018 June 30
GJI Marine geosciences and applied geophysics

doi: 10.1093/gji/ggy262

# Waves at fluid–solid interfaces: explicit versus implicit formulation of the boundary condition

José M. Carcione,[1] Claudio Bagaini,[2] Jing Ba,[3] Enjiang Wang[3] and Aldo Vesnaver[4]

[1] *Istituto Nazionale di Oceanografia e di Geofisica Sperimentale (OGS), Borgo Grotta Gigante* 42c, 34010 *Sgonico, Trieste, Italy*
[2] *Schlumberger, Gatwick* RH6 0NZ, *UK*
[3] *School of Earth Science and Engineering, Hohai University, Nanjing* 211100, *China. E-mail: jba@hhu.edu.cn*
[4] *Petroleum Geoscience Department, Petroleum Institute, Khalifa University of Science and Technology,* P.O. Box 2533, *Abu Dhabi, United Arab Emirates*

Accepted 2018 June 29. Received 2018 January 24; in original form 2018 June 25

## SUMMARY

The correct simulation of wave propagation with direct grid methods at fluid–solid interfaces requires a proper implementation of the boundary condition, which involves continuity of the normal component of the particle velocity and traction. The horizontal component of the particle velocities can differ (slip) and the tangential traction vanishes. The challenge is to model the interface waves, which are relevant when the source and receiver are located close to the interface, in particular the Scholte and leaky (or pseudo, or generalized) Rayleigh waves. The explicit modelling is based on a domain-decomposition technique (one mesh for the fluid and another mesh for the solid) and the Fourier and Chebyshev differential operators along the horizontal and vertical directions, respectively. On the other hand, two implicit modelling algorithms are based on a single mesh and the fluid is described by setting to zero the shear wave velocity above the interface. The modelling is verified by comparisons with the analytical solution for a fluid–solid interface in lossless media, with source and receiver away from and at the interface. To our knowledge, the latter comparison, mainly involving the interface waves (Scholte and leaky-Rayleigh), has not been performed with other grid methods so far. It is shown that the implicit simulation yields erroneous results.

**Key words:** Elasticity and anelasticity; Numerical modelling; Body waves; Interface waves; Wave propagation.

## 1 INTRODUCTION

The problem of reflection, refraction and propagation of waves at a plane boundary separating an acoustic medium (fluid) and an elastic solid has practical application in seismic exploration, seismology, foundation engineering and other fields of research (e.g. Roever *et al.* ; Brekhovskikh & Lysanov 1991). In offshore seismic exploration, the relevant fluid–solid interface is the ocean bottom, whose properties are useful for data processing of multicomponent seismic surveys acquired at the seafloor.

In some situations, there exist two interface waves at a fluid–solid interface, one that travels mainly in the liquid and the other that has most of its energy in the solid. Cagniard (1962) investigated the first type of waves, suggesting to call them 'Scholte waves'. The second is a leaky-Rayleigh wave, propagating along the interface (Auld 1985). The leaky-Rayleigh wave at a lossless fluid–solid interface decays with depth in the bottom but corresponds to a propagating body wave in the fluid (with characteristics similar to head waves). The amplitude of this wave increases in the fluid away from the interface (Farnell 1970; Auld 1985; Lord Rayleigh discarded these solutions on the basis of this behaviour). Leaky-Rayleigh waves can explain arrivals of supersonic waves observed in the Canadian Artic (Chamuel 1991).

Padilla *et al.* (1999) and Glorieux *et al.* (2001, 2002) describe the main physical aspects of the problem, with divergent statements. It can be summarized as follows: (1) When the fluid sound velocity $c_f$ is lower than the velocities of the bulk shear wave $c_S$ and the bulk longitudinal wave $c_L$ in the solid, the leaky-Rayleigh wave propagates with a phase velocity $c_{\rm pR}$ slightly lower than $c_S$ and radiates energy into the fluid (it is leaking energy into the fluid in the form of a head wave). The Stoneley (Scholte) wave phase velocity $c_{\rm Sc}$ is lower than the velocities in the two media; (2) according to Padilla *et al.* (1999), when $c_S < c_f < c_L$ the Rayleigh root becomes real (the wave is not leaking energy into the fluid). Glorieux *et al.* (2001) show that this root has been incorrectly identified as the leaky-Rayleigh wave in Padilla *et al.* (1999) and that it is not physical; (3) when the density of the fluid decreases to zero, the Scholte–Stoneley equation becomes the Rayleigh-wave equation and the leaky-Rayleigh wave becomes a free Rayleigh wave; (4) in the case of a large acoustic impedance mismatch between solid and liquid, the Scholte velocity lies very close to $c_f$; (5) for softer solids, or equivalently, less compressible liquids, the Scholte wave becomes

more localized and slows down compared to the liquid bulk velocity; (6) because there is no leakage during Scholte wave propagation along the radial direction in 3-D, the decay in the radial direction is only attributed to the geometrical effect. In 2-D cases, the Scholte wave travels without attenuation along the propagation direction. The inequalities $c_{\rm Sc} < c_R < c_{\rm pR} < c_f < c_S < c_L$ hold for a stiff solid, where $c_R$ is the free Rayleigh wave velocity in the solid. The front of the leaky part of the Rayleigh wave (the head wave in the fluid) makes an angle with the normal to the interface called the Rayleigh angle: $\cos^{-1}(c_L/c_R)$, which is the incidence angle at which the Rayleigh window exists at a fluid-viscoelastic solid interface (Carcione & Helle 2004; Carcione 2006).

To our knowledge, Stephen (1983) was the first to model waves at a fluid–solid interface using direct grid methods, specifically a finite-difference algorithm. He first treated the boundary condition explicitly up to second order. He clearly states: 'The boundary conditions for a liquid–solid interface are fundamentally different from the conditions for a solid–solid interface and although letting the shear modulus go to zero in the solid–solid calculations may produce stable and apparently good results the seismograms are incorrect.' Alternatively, if the interface is represented by a transition zone (a ramp discontinuity), that is, a gradual change, there is no apparent stability problem with the heterogeneous formulation and it is not necessary to introduce the interface boundary condition explicitly. Stephen (1988) shows simulations using the transition zone, where all the wave types at a fluid–solid interface are illustrated. Komatitsch *et al.* (2000) have developed a spectral finite element approach to explicitly model the boundary condition. Similarly, van Vossen *et al.* (2002) present an explicit method and show that only five grid points per wavelength are needed for accurate calculations with the finite-difference method. Zhang (2004) explicitly models the boundary condition using an integral approach and unstructured mesh. Besides Stephen (1988), all the previous methods mentioned above do not show the propagation of the interface waves, namely, the Scholte and the leaky-Rayleigh waves, and all the formulations have not been compared to an analytical solution. Carbajal-Romero *et al.* (2013) employ a boundary element method to simulate body and Scholte waves and validate their results by using the discrete wave-number method and the spectral-element method but do not model the complete set of waves observed (the leaky-Rayleigh wave is missing). Chaljub *et al.* (2003) simulate waves in a heterogeneous fluid–solid sphere with a spectral-element method, where the boundary conditions are explicitly satisfied. Comparisons with a reference solution are optimal, but they do not simulate the interface waves treated in the present paper. Madec *et al.* (2009) use high-order finite elements to solve the problem, but do not consider those interface waves either. The work by Wilcox *et al.* (2010), based on a discontinuous Galerkin method, treats the problem in general but, again, there are no simulations of those interface waves and/or comparison with analytical solutions. Similarly, Caiman *et al.* (2011) establish an explicit continuity of velocity and traction along fluid–solid interfaces, but the nature of the problem is different from ours.

Recently, De Basabe & Sen (2015) effectively show how difficult is to correctly simulate interface waves without an explicit modelling of the fluid–solid boundary conditions. They have compared the results obtained with several algorithms, including finite-difference and spectral-element methods. For instance, their fig. 21 shows various degrees of accuracy to model the Scholte wave, but all of the considered methods yield a limited accuracy. They conclude that single-grid (so-called monolithic) methods have spurious modes in the fluid subdomain, explained by the fact that an elastic formulation is implemented for the fluid. They do not show comparisons by using an explicit implementation of the boundary conditions.

Carcione & Helle (2004) and Zhu *et al.* (2004) perform a complete (full-wave) modelling of the Scholte & Rayleigh waves and compared their results to an analytical solution. Zhu *et al.* (2004) have used the elastodynamic finite integration technique algorithm, which treats explicitly the fluid–solid boundary condition. Carcione & Helle (2004) used a domain-decomposition method and model the whole set of waves at the interface by using pseudospectral differential operators. They also include anelasticity and study its effects on wave propagation, such as the Rayleigh window. Interface waves are exponentially damped away from the interface, so they require denser grid points than body waves. Therefore, an accurate simulation of interface waves requires, in general, a special boundary treatment, particularly when using finite-difference (e.g. Mittet 2002) and pseudospectral methods. Here, we use a domain-decomposition method based on pseudospectral differential operators to model explicitly the boundary conditions. The implicit modelling employs one mesh and the fluid is described by setting to zero the shear-wave velocity above the interface. Both approaches use the Fourier method along the interface direction and the Chebyshev method along the direction perpendicular to the interface. In the implicit case a vertical mapping transformation (Carcione. 2000) stretches the mesh at the boundaries and defines denser grid points at the centre, where the fluid–solid interface is located. An additional implicit algorithm based on the staggered Fourier pseudospectral method (regular cells) is also tested (Carcione 1999).

The paper is organized as follows. The first sections provide the theory. Then, the domain-decomposition method for anelastic fields is described. Next, we present the results for the interface waves, including a test of the modelling algorithm and the analysis of the physics.

## 2 EQUATION OF MOTION

The time-domain equations for wave propagation in a heterogeneous elastic medium can be found in Carcione (2014). The two-dimensional velocity–stress equations for elastic wave propagation in the $(x, z)$-plane can be expressed by

(i) Euler–Newton's equations:

$$\dot{v}_x = \frac{1}{\rho}(\sigma_{xx,x} + \sigma_{xz,z}), \tag{1}$$

$$\dot{v}_z = \frac{1}{\rho}(\sigma_{xz,x} + \sigma_{zz,z}), \tag{2}$$

where $v_x$ and $v_z$ are the particle velocities, $\sigma_{xx}$, $\sigma_{zz}$ and $\sigma_{xz}$ are the stress components and $\rho$ is the density. A dot above a variable denotes time differentiation, and the subindices ', $x$' and ', $z$' indicate spatial derivatives with respect to the Cartesian coordinates.

(ii) Constitutive equations:

$$\dot{\sigma}_{xx} = k(v_{x,x} + v_{z,z}) + \mu(v_{x,x} - v_{z,z}) + f_{xx}, \tag{3}$$

$$\dot{\sigma}_{zz} = k(v_{x,x} + v_{z,z}) - \mu(v_{x,x} - v_{z,z}) + f_{zz}, \tag{4}$$

$$\dot{\sigma}_{xz} = \mu(v_{x,z} + v_{z,x}) + f_{xz}, \tag{5}$$

where $k$ and $\mu$ are the bulk and shear moduli, respectively, and $f_{ij}$ are moment forces. In 2-D space, $k = \rho(c_L^2 - c_S^2)$ and $\mu = \rho c_S^2$, where $c_L$ and $c_S$ are the $P$- and $S$-wave velocities, respectively.

The equations for the acoustic medium (fluid) are obtained from eqs (1)–(5) by setting $\sigma_{xx} = \sigma_{zz} \equiv \sigma$, $\sigma_{xz} = 0$ and $\mu = 0$. Then,

$$\dot{v}_x = \frac{\sigma_{,x}}{\rho_f}, \quad \dot{v}_z = \frac{\sigma_{,z}}{\rho_f}, \tag{6}$$

where $\rho_f$ is the fluid density and

$$\dot{\sigma} = k(v_{x,x} + v_{z,z}) + s, \tag{7}$$

where $k = \rho_f c_f^2$ and $s$ is an explosion source.

## 3 THE DISPERSION EQUATION

The dispersion equation is obtained by requiring continuity of the normal components of the displacement and stress at the interface. Details can be found in Scholte (1942), Glorieux *et al.* (2001, 2002) and Carcione & Helle (2004). Let us define

$$q = \frac{v^2}{c_S^2}, \quad a = \frac{c_S^2}{c_L^2}, \quad b = \frac{c_S^2}{c_f^2}, \tag{8}$$

where $v$ is the complex velocity of the interface waves. The dispersion equation can be expressed as

$$S(q) = 4\sqrt{1-q}\sqrt{1-aq} - (2-q)^2 - \left(\frac{\rho_f}{\rho}\right) q^2 \sqrt{\frac{1-aq}{1-bq}} = 0 \tag{9}$$

(Brekhovskikh & Lysanov 1991, p. 67). If $\rho_f = 0$, this equation reduces to the dispersion equation for elastic Rayleigh waves (e.g. Carcione 2014). Ansell (1972) obtained the roots of the dispersion equation by a detailed analysis in the complex wavenumber plane (see Padilla *et al.* 1999). The Riemann surface of function $S$ has eight sheets, which correspond to different choices of the signs of the complex square roots $\sqrt{1-q}$, $\sqrt{1-aq}$ and $\sqrt{1-bq}$. In the lossless elastic case, roots of the Scholte wave are real, while the roots of the leaky-Rayleigh wave are complex. Thus, the first wave travels without attenuation and the second decays along the interface. These surface waves are superpositions of inhomogeneous elastic waves, that is, the attenuation vector makes an angle of 90° with respect to the propagation vector. For Scholte waves, the attenuation vector is perpendicular to the interface, while for leaky-Rayleigh waves, the attenuation vector has a non-zero projection on the interface.

In general, there are five causes of amplitude reduction: geometrical spreading, evanescent decay (diffraction), leaking, intrinsic energy loss and scattering. The term decay can be used for all the cases, but the term attenuation applies to the last two causes. In the lossless 2-D case, the Scholte wave travels without attenuation because it is not a leaky mode, but in 3-D space it would decay because of geometrical spreading. On the other hand, the leaky-Rayleigh wave decays for lossless media in both 2-D and 3-D media.

The existence of the leaky wave is subject to the condition that the sound velocity in the liquid must be less than the shear velocity in the solid. The leaky-Rayleigh wave approaches the Rayleigh wave as the density of the liquid tends to zero. Hence, the Rayleigh wave in a vacuum solid interface is not the Scholte wave when the density of the liquid goes to zero. This applies to the stiff bottom case (shear velocity higher than the sound velocity in water). On the other hand, for the soft bottom case (shear velocity less than water velocity), the Scholte wave pole converges to the Rayleigh pole as the density of the water goes to zero (Rauch 1980). While the free Rayleigh wave always exists, the leaky-Rayleigh wave does not (Brower *et al.* 1979). Most quasi-surface waves, corresponding to roots lying on lower Riemann sheets, are not always physically separable on experimental or numerical simulations due to their close association with body-wave phases. For instance, Phinney (1961) predicts a pseudo-$P$ pulse coupled to the $P$ wave.

For a stiff fluid–solid interface, the leaky-Rayleigh wave has a velocity slightly lower than the body-wave shear velocity, and the Scholte wave velocity is lower than the liquid sound velocity. As the solid becomes stiffer, the Scholte wave velocity approaches that of the liquid. The leaky-Rayleigh wave is also relevant in wave propagation in boreholes (Paillet & White 1982).

**Table 1.** Properties of body and surface waves.

| Interface | $c_f$ ($m\,s^{-1}$) | $\rho_f$ ($kg\,m^{-3}$) | $c_L$ ($m\,s^{-1}$) | $c_S$ ($m\,s^{-1}$) | $\rho$ ($kg\,m^{-3}$) | $c_{Sc}$ ($m\,s^{-1}$) | $c_{pR}$ ($m\,s^{-1}$) |
|---|---|---|---|---|---|---|---|
| Water–plexiglas | 1500 | 1000 | 2745 | 1390 | 1180 | 1058 | 1363 |
| Water–glass | 1500 | 1000 | 5712 | 3356 | 2500 | 1496 | 3091 |

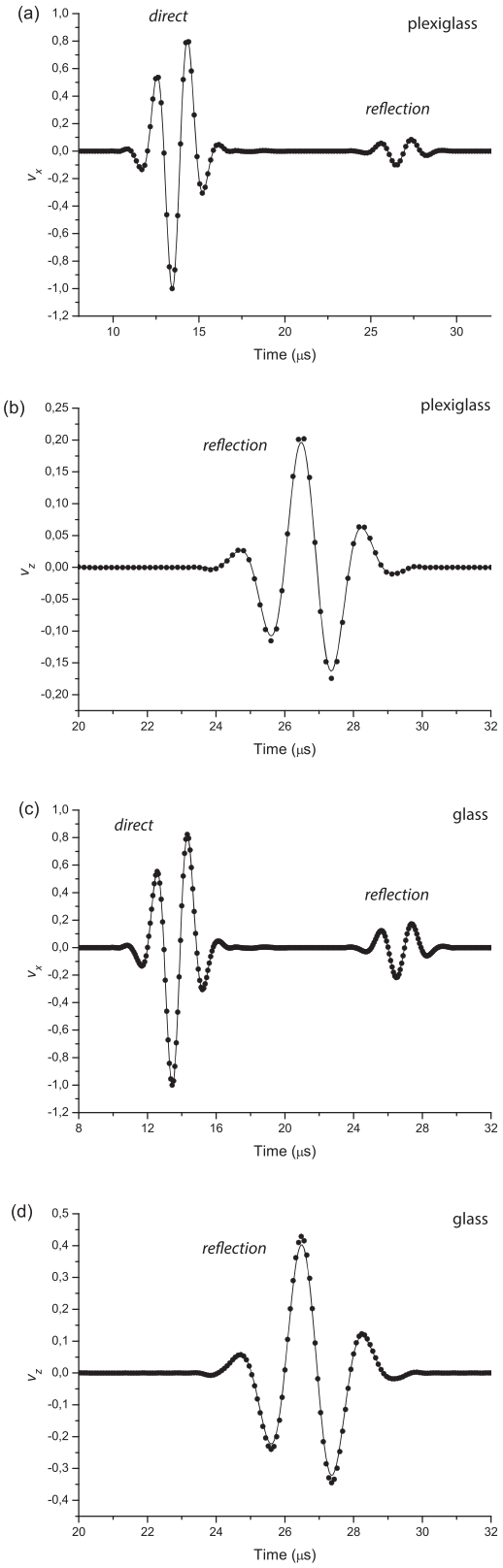


**Figure 1.** Explicit boundary-condition reflection simulation, where the solid line and dots correspond to the analytical and numerical solutions, respectively. The figure shows the normalized particle–velocity components corresponding to water–plexiglass (a and b) and water–glass (c and d). Source and receiver are both located in the fluid at 0.0158831 m above the interface and are separated by 0.016 m. The source is an explosion, with a central frequency of 500 kHz.

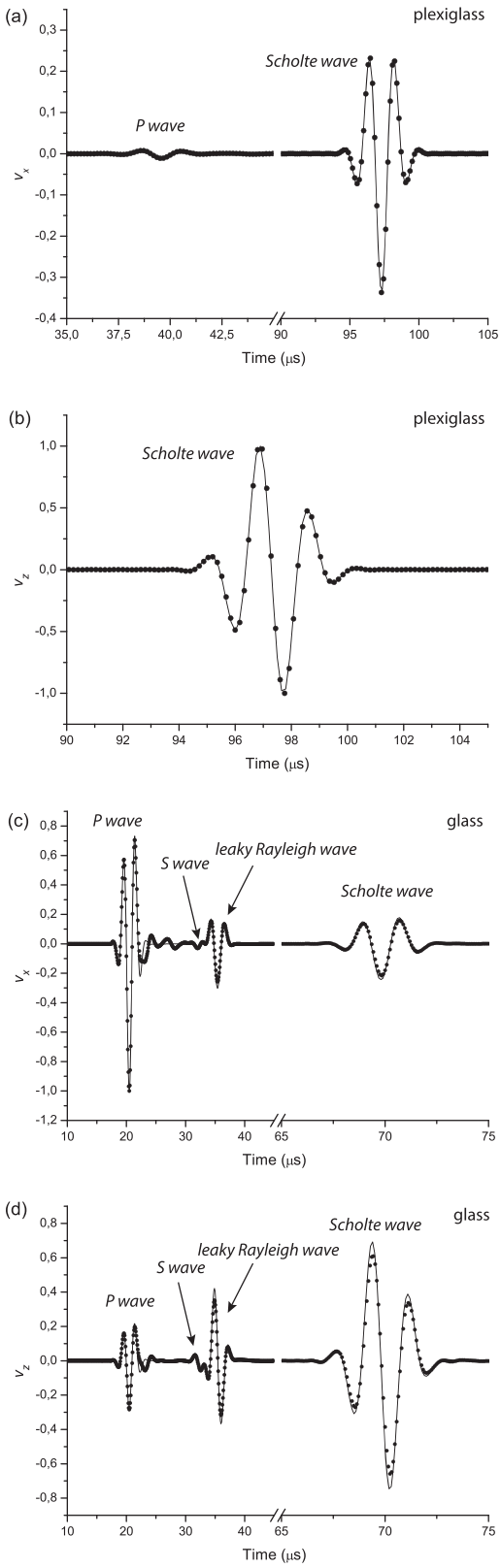


**Figure 2.** Explicit boundary-condition interface-wave simulation, where the solid line and dots correspond to the analytical and numerical solutions, respectively. The figure shows the normalized particle–velocity components corresponding to water–plexiglass (a and b) and water–glass (c and d). Source and receiver are both located in the solid at 38.4 μm below the interface and are separated by 0.1 m. The source is an explosion ($f_{xx} = f_{zz}$), with a central frequency of 500 kHz.

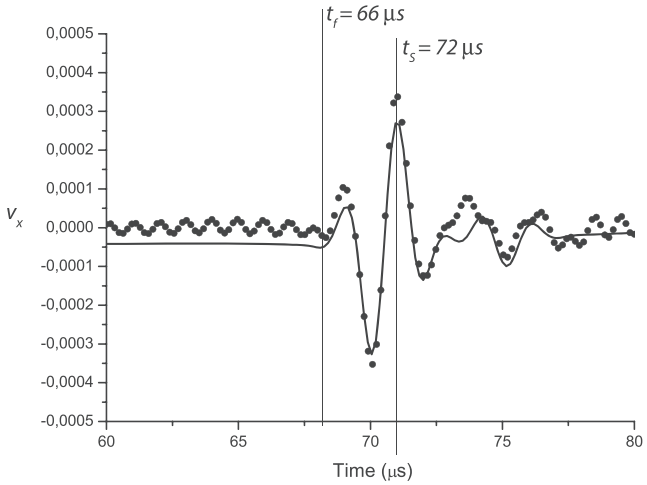


**Figure 3.** Explicit boundary-condition interface-wave simulation, where the solid line and dots correspond to the analytical and numerical solutions, respectively. The figure shows the horizontal particle–velocity component corresponding to water–plexiglass (Fig. 2a). The arrival times of the main events are indicated. Compared to Fig. 2(a), the field has been enhanced by a factor 2000.

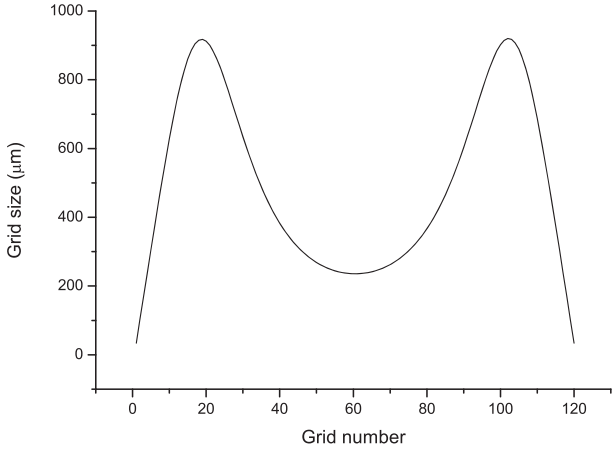


**Figure 4.** Grid size as a function of the grid number for the single mesh used in the heterogeneous algorithm.

## 4 MODELLING TECHNIQUES

### 4.1 Implicit modelling

This approach uses a single mesh and describes the fluid by setting to zero the shear-wave velocity. The solution is obtained by using the Runge–Kutta method as time stepping algorithm and the Fourier and Chebyshev differential operators to compute the spatial derivatives in the horizontal and vertical directions, respectively (Carcione 1992; Carcione 2014).

The uneven distribution of points of the Chebyshev differential operator has two main disadvantages. In the first place, the stability condition and the accuracy of the time integration scheme depend on the minimum grid spacing of the mesh. The dense concentration of points of the Chebyshev mesh at the boundaries requires very small time steps, making the modelling algorithm highly inefficient. In second place, there is no justification for concentrating points in regions where there are not small inhomogeneities to model. In this sense, grid adaptation is fully justified. These problems are solved by expanding the solution as a finite sum of non-polynomial basis functions. This is achieved by 1-D transformations or stretching functions which are applied to the Gauss–Lobatto points and yield a numerical grid that can be adapted to the particular structure of the model and boundary conditions. Along the $z$-direction, a non-symmetric stretching function with denser grid at the centre is used, in order to sample the wavefield appropriately to model the boundary condition, but coarse enough to avoid the severe stability condition.

We consider the following coordinate transformation from the computational to the physical domain:

$$z_j = z_{\max}\left[\frac{q(\zeta_j)-q(1)}{q(-1)-q(1)}\right], \quad j = 0, \ldots, N \tag{10}$$

mapping the interval $[1,-1]$ onto the interval $[0\ , z_{\max}]$, such that the physical domain is $(x, z) \in [\ 0, x_{\max}] \times [\ 0, z_{\max}]$. The function

$$q = q(\zeta, \boldsymbol{\alpha}) \tag{11}$$

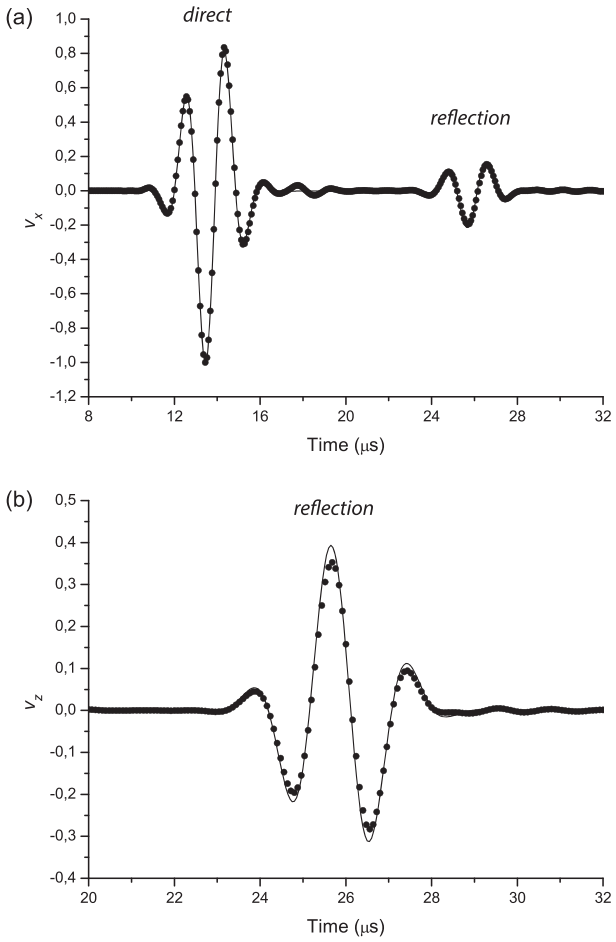


**Figure 5.** Reflection simulation, where the solid line and dots correspond to the analytical and numerical solutions, respectively. The figure shows the normalized particle–velocity components corresponding to water–glass (a and b), for the heterogeneous (implicit) formulation of the fluid–solid boundary condition. Source and receiver are both located in the fluid at 0.0151776 m above the interface and are separated by 0.016 m. The source is an explosion , with a central frequency of 500 kHz.

is a family of transformations, where $\boldsymbol{\alpha}$ is a vector of parameters defining the mapping.

The spatial derivative of a field variable $u$ in the physical domain is then given by

$$\frac{\partial u}{\partial z} = \frac{\partial u}{\partial \zeta}\frac{\mathrm{d}\zeta}{\mathrm{d}z} = \left[\frac{q(-1) - q(1)}{z_{\max}}\right]\frac{\mathrm{d}\zeta}{\mathrm{d}q}\frac{\partial u}{\partial \zeta}. \tag{12}$$

A non-symmetric transformation is

$$q(\zeta) = \frac{\pi\delta - 2p}{2p\delta - \pi}, \quad p = \arctan\left[\epsilon \tan\left(\frac{\pi\zeta}{2}\right)\right], \tag{13}$$

with $\boldsymbol{\alpha} = (\delta, \epsilon)$ and

$$\frac{\mathrm{d}\zeta}{\mathrm{d}q} = \frac{(2p\delta - \pi)^2}{\pi^2\epsilon(1-\delta^2)}\left[\cos^2\left(\frac{\pi\zeta}{2}\right) + \epsilon^2 \sin^2\left(\frac{\pi\zeta}{2}\right)\right], \tag{14}$$

where $\epsilon > 0$ and $|\delta| < 1$. The parameter $\epsilon$ controls the magnitude of the coordinate stretching (or compression) about a point determined by $\delta$. For $\zeta = \pm 1$ the amount of stretching is given by

$$\frac{\mathrm{d}\zeta}{\mathrm{d}q} = \frac{1 \mp \delta}{1 \pm \delta}\epsilon. \tag{15}$$

### 4.2 Explicit modelling

In this case, two meshes model the fluid and solid subdomains (labelled 1 and 2, respectively). The solution on each mesh is obtained by using the previous techniques. In order to combine the two grids, the wave field is decomposed into incoming and outgoing wave modes at the interface between the solid and the fluid. The inward propagating waves depend on the solution exterior to the subdomains and therefore

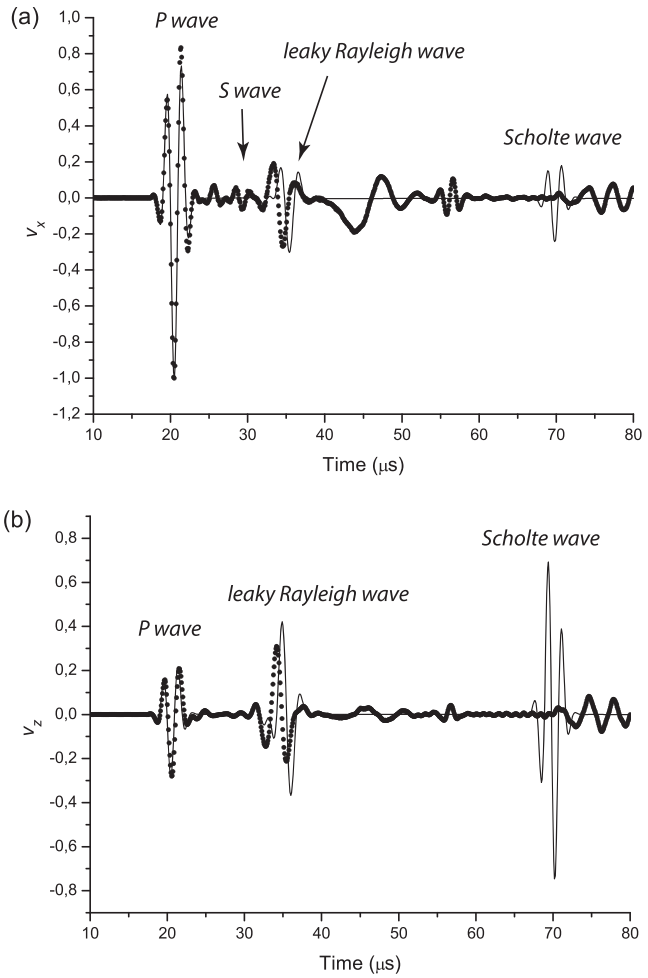


**Figure 6.** Interface-wave simulation, where the solid line and dots correspond to the analytical and numerical solutions, respectively. The figure shows the normalized particle–velocity components corresponding to water–glass (a and b), for the heterogeneous (implicit) formulation of the fluid–solid boundary condition, based on the Chebyshev pseudospectral method. Source and receiver are both located in the solid at 118.15 μm below the interface and are separated by 0.1 m. The source is an explosion ($f_{xx} = f_{zz}$), with a central frequency of 500 kHz.

are computed from the boundary conditions, while the behaviour of the outward propagating waves is determined by the solution inside the subdomain (e.g. Carcione 2014). The approach involves the following equations for updating the field variables at the grid points defining the fluid–solid interface:

$$
\begin{aligned}
&v_x^{(\mathrm{new})}(1) = v_x^{(\mathrm{old})}(1),\\
&v_z^{(\mathrm{new})}(1) = v_z^{(\mathrm{new})}(2) = [Z_P(1) + Z_P(2)]^{-1}[Z_P(2)v_z^{(\mathrm{old})} + Z_P(1)v_z^{(\mathrm{old})} + \sigma^{(\mathrm{old})}(1) - \sigma_{zz}^{(\mathrm{old})}(2)],\\
&\sigma^{(\mathrm{new})}(1) = \sigma_{zz}^{(\mathrm{new})}(2) = \frac{Z_P(1)Z_P(2)}{Z_P(1) + Z_P(2)}\left[v_z^{(\mathrm{old})}(1) - v_z^{(\mathrm{old})}(2) + \frac{\sigma^{(\mathrm{old})}(1)}{Z_P(1)} + \frac{\sigma_{zz}^{(\mathrm{old})}(2)}{Z_P(2)}\right],\\
&v_x^{(\mathrm{new})}(2) = v_x^{(\mathrm{old})}(2) - \sigma_{xz}^{(\mathrm{old})}(2)/Z_S(2),\\
&\sigma_{xz}^{(\mathrm{new})}(2) = 0,\\
&\sigma_{xx}^{(\mathrm{new})}(2) = \sigma_{xx}^{(\mathrm{old})}(2) + \frac{k(2) - \mu(2)}{k(2) + \mu(2)}[\sigma_{zz}^{(\mathrm{new})}(2) - \sigma_{zz}^{(\mathrm{old})}(2)],
\end{aligned}
\tag{16}
$$

where $Z_P(1) = \rho_f c_f$, $Z_P(2) = \rho c_L$ and $Z_S(2) = \rho c_S$ are impedances (Carcione & Helle 2004).

The upper boundary of subdomain 1 (the fluid) may satisfy free-surface or non-reflecting boundary conditions (Carcione & Helle 2004). In addition to the non-reflecting conditions, absorbing strips are used to further attenuate the wave field at non-physical boundaries (Carcione 2014).

The modelling algorithm can be applied to a non-planar interface by using a curvilinear mapping that transforms the physical domain into a rectangular computational domain where the spatial derivatives are calculated with the pseudospectral Fourier and Chebychev methods (Carcione 1994).

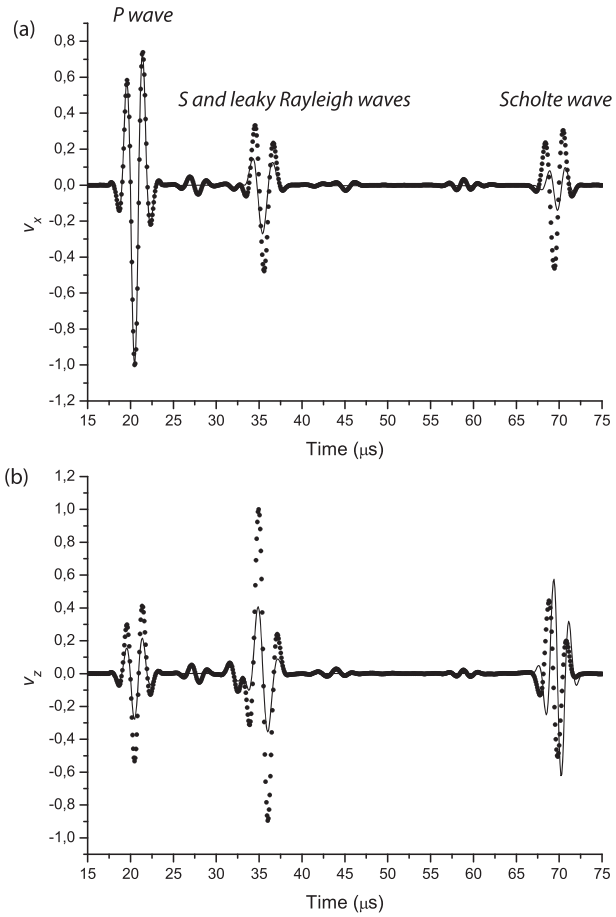


**Figure 7.** Interface-wave simulation, where the solid line and dots correspond to the analytical and numerical solutions, respectively. The figure shows the normalized particle–velocity components corresponding to water–glass (a and b), for the heterogeneous (implicit) formulation of the fluid–solid boundary condition, based on the staggered Fourier method. Source and receiver are both located in the solid at 100 μm below the interface and are separated by 0.1 m. The source is an explosion ($f_{xx} = f_{zz}$), with a central frequency of 500 kHz.

## 5 COMPARISON OF NUMERICAL AND ANALYTICAL SOLUTIONS

Interface waves at liquid–solid boundaries have been investigated with some detail in the field of non-destructive testing of materials, where the experiments are performed in the ultrasonic range (Roever *et al.* ). The research performed in this field is relevant for seismic exploration and geotechnical applications. We consider the two interfaces given in Table 1. The velocities of the Scholte wave ($c_{\rm Sc}$) and leaky-Rayleigh wave ($c_{\rm pR}$) are indicated. The first wave corresponds to the choice (+, +, +) for the signs of $\sqrt{1-q}\sqrt{1-aq}$ and $\sqrt{1-bq}$, while the second surface wave corresponds to a lower sheet with the choice (+, −, +). Roots in lower sheets such as (1878,−24) m s$^{-1}$ and (2097,97) m s$^{-1}$ are physically impermissible steady-state waves, but the result of superposition in the time domain may be physically reasonable (Phinney 1961).

As shown by Glorieux *et al.* (2002) from laboratory experiments and by our simulations (see below), the real solution $c_{\rm pR} = 1363$ m s$^{-1}$ is not a physical solution, which has been identified by Padilla *et al.* (1999) as an unleaky-Rayleigh wave. On the other hand, the corresponding solution for the water–glass interface is a complex physical solution with value (3091,−109) m s$^{-1}$.

We test the numerical solution against the analytical solution obtained by Berg *et al.* (1994) using the method of Cagniard-de Hoop (de Hoop & van der Hijden 1983). Let us first consider the simulation of wave propagation with the explicit formulation. Each mesh has 405 × 81 points with a horizontal grid spacing of 0.5 mm and a vertical size of 30 mm. The source is a dilatational moment force ($f_{xx} = f_{zz}$ and $f_{xy} = 0$) with a dominant frequency of 500 kHz.

The time history of the source is a Ricker wavelet with a central peak frequency $f_p$:

$$h(t) = \exp\left[-2f_p^2(t-t_0)^2\right]\cos[2\pi f_p(t-t_0)], \tag{17}$$

where $t_0 = 3/(4f_p)$.

For the reflection problem, source and receiver are both located in the fluid at 0.0158831 m = 15 883.1 μm above the interface, and are separated by 0.016 m. Besides the non-reflecting condition, 40 grid points are used as absorbing boundary at the sides, top and bottom of the grids. The time step is 40 ns for water–plexiglas and 20 ns for water–glass. Fig. 1 shows comparisons of the numerical and analytical solutions, corresponding to the water–plexiglas interface (a and b) and water–glass interface (c and d). The agreement between solutions for the horizontal and vertical particle components of the particle velocity is very good.

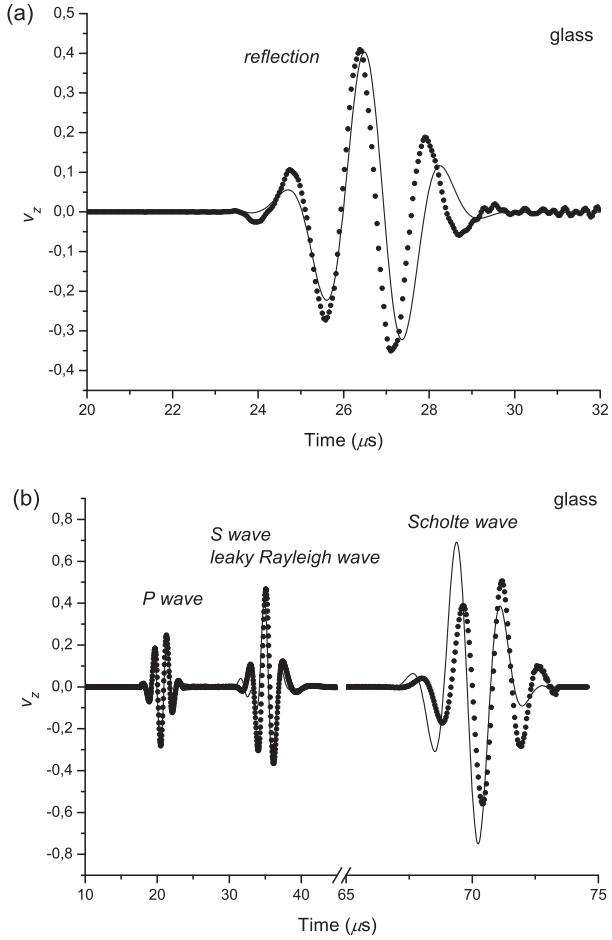


**Figure 8.** Results obtained with a staggered finite-difference code corresponding to (a) the reflection problem, equivalent to that of Figs 1(d), and (b) the interface-wave simulation, equivalent to that of Fig. 2(d).

Next, we verify the ability of the algorithm to model interface waves. Source and receiver are both located in the solid at 38.4 μm below the interface, and are separated by 0.1 m. The numerical and analytical solutions are compared in Fig. 2, where it is clear that the agreement is satisfactory. Fig. 3 shows the horizontal particle velocity in the solid between 60 and 80 $\mu$s. The arrival times of the *P* wave in the fluid and the *S* wave in the solid are indicated. Compared to Fig. 2(a), the field has been enhanced by a factor 2000, but the algorithm still reproduces the very weak P and S waves fairly well. These comparisons confirm the accuracy of the modelling algorithm to model the interface waves.

The following simulations consider the heterogeneous formulation for the water–glass case, that is, the boundary condition is implicitly modelled by setting the shear-wave velocity of the upper medium (water) equal to zero. We use one mesh with 405 × 121 cells, whose vertical grid points are determined by the mapping transformation (13), with $\delta = 0$ and $\epsilon = 0.3$. The size of the cells as a function of depth is shown in Fig. 4. As can be seen, the grid size has a minimum at the location of the fluid–solid interface, between grid numbers 59 and 60, which correspond to water and glass, respectively. The interface is located in the middle at 118.15 μm above grid 60. The source and receiver are placed at grid 24 at 15 177.65 μm above the interface. In this case, twenty grid points are used as absorbing boundary at the sides, top and bottom of the grids. The comparison between the numerical and analytical solutions for the reflection problem is shown in Fig. 5. The numerical solution performs well but without the accuracy of the domain-decomposition algorithm (see Figs 1c and d).

Next, we locate the source and receiver at grid point 60, that is, 118.15 μm below the interface, and separated by 0.1 m. Fig. 6 shows the comparison between the analytical and numerical solutions (compare to Fig. 2). The body waves seem to be simulated fairly well but the interface waves (leaky-Rayleigh and Scholte) are not correct. We have increased the number of vertical grid points to 289 in order to have a denser grid at the interface (comparable to that of the domain-decomposition grid) but the numerical solution (not shown) did not improved .

It is well known that the computation of spatial derivatives using staggered grids removes strong numerical artefacts in the form of non-causal ringing in pseudospectral methods (Carcione 1996). Staggered grids also improve the performance of finite-difference methods (Zhu *et al.* 2004). In the following, we have attempted to solve the water–glass problem using the implicit method in Carcione (1996), based on the staggered Fourier pseudospectral method. The mesh is regular along the horizontal and vertical coordinates with a cell size of 333.33 μm and 200 μm, respectively and 616 × 616 grid points. The source and receiver (in the solid) are located at 100 μm below the fluid–solid interface. As above, the dominant frequency is 500 kHz, with a time step of 0.02 $\mu$s. Fig. 7 shows the comparison between the analytical and numerical solutions for $v_x$ and $v_z$. The P wave reproduces well in the horizontal component but the other events do not, despite that the arrival

times seem to be correct. We have verified (not shown here) that the Scholte wave is not modelled correctly with the implicit formulation in the soft-solid case as well (e.g. water–plexiglass).

In order to further verify that the heterogeneous (implicit) formulation does not yield accurate results, we have tested a modelling code based on staggered finite differences to solve the velocity–stress equations (van Vossen *et al.* 2002). The mesh has 1150 × 200 points (with 20 grid points for absorbing boundaries) and the grid spacings are 200 and 159 μm (reflection problem) and 100 μm and 77 μm (interface-wave problem) along the horizontal and vertical directions, respectively. The time steps are 0.01 $\mu$s and 0.004 μs, respectively. We have considered the hard-solid case, where pseudo-Rayleigh wave is present. Fig. 8 shows (a) the reflection problem, equivalent to that of Figs 1(d), and (b) the interface-wave simulation, equivalent to that of Fig. 2(d). The results show that the algorithm cannot properly reproduce the events. We have also verified (not shown here) that the Scholte wave is not modelled correctly with the implicit formulation in the soft-solid case.

## 6 CONCLUSIONS

Almost all the publications dealing with the simulation of waves at the fluid–solid interface and its applications, mainly performed with finite-difference algorithms and their staggered-grid versions using a single mesh, do not show the complete set of waves (i.e. including the Scholte and leaky-Rayleigh waves) and a comparison with the analytical solution has not been performed. This test is essential to verify the correct simulation in the presence of a such interface. We present in this work analytical and numerical results for the simulation of waves propagating at the fluid–solid interface for two solids: plexiglas and glass. In the case of glass, which is a stiff solid whose shear wave velocity is more than twice the fluid sound velocity (e.g. a stiff ocean bottom), the numerical solution is in excellent agreement with the analytical solution if a domain decomposition approach is used with an explicit definition of the boundary conditions. If a single domain with implicit boundary conditions is used, neither the kinematics nor the dynamic of interface waves (Scholte and leaky-Rayleigh waves) are correctly modelled.

## 7 ACKNOWLEDGEMENTS

This work is supported by Specially-Appointed Professor Program of Jiangsu Province, China, the Cultivation Program of "111" Plan of China (BC2018019) and the Fundamental Research Funds for the Central Universities, China.

## REFERENCES

Ansell, J.H., 1972. The roots of the Stoneley wave equation for liquid-solid interfaces, *Pure appl. Geophys.,* **94,** 172–188.

Auld, B.A., 1985. Rayleigh wave propagation, in *Rayleigh-Wave Theory and Application,* pp. 12–27, eds Ash, E.A. & Paige, E.G.S., Springer-Verlag.

Berg, P., If, F., Nielsen, P. & Skovgaard, O., 1994. Analytical reference solutions, in *Modeling the Earth for Oil Exploration,* pp. 421–427, ed. Helbig, K., Pergamon Press.

Brekhovskikh, L.M. & Lysanov, Y.P., 1991. *Fundamentals of Ocean Acoustics,* Springer-Verlag.

Brower, N.G., Himberger, D.E. & Mayer, W.G., 1979. Restrictions on the existence of leaky Rayleigh waves, *IEEE Trans. Sonics and Ultrason.,* **26,** 306–308.

Cagniard, L., 1962. *Reflection and Refraction of Progressive Seismic Waves,* McGraw-Hill Book Co., Inc.

Carbajal-Romero, M., Flores-Mendez, E., Flores-Guzmán, N., Núñez-Farfán, J., Olivera-Villaseñor, E. & Sánchez-Sesma, F.J., 2013. Scholte waves on fluid-solid interfaces by means of an integral formulation, *Geofis. Int.,* **52,** 21–30.

Carcione, J.M., 1992. Modeling anelastic singular surface waves in the Earth, *Geophysics,* **57,** 781–792.

Carcione, J.M., 1994. The wave equation in generalized coordinates, *Geophysics,* **59,** 1911–1919.

Carcione, J.M., 1996. A 2-D Chebyshev differential operator for the elastic wave equation, *Comput. Methods Appl. Mech. Eng.,* **130,** 33–45.

Carcione, J.M., 1999. Staggered mesh for the anisotropic and viscoelastic wave equation, *Geophysics,* **64,** 1863–1866.

Carcione, J.M., 2006. Vector attenuation: elliptical polarization, raypaths and the Rayleigh-window effect, *Geophys. Prospect.,* **54,** 399–407.

Carcione, J.M., 2014. *Wave Fields in Real Media. Theory and Numerical Simulation of Wave Propagation in Anisotropic, Anelastic, Porous and Electromagnetic Media,* 3rd edn, Elsevier.

Carcione, J.M. & Helle, H.B., 2004. On the physics and simulation of wave propagation at the ocean bottom, *Geophysics,* **69,** 825–839.

Chaljub, E., Capdeville, Y. & Vilotte, J.P., 2003. Solving elastodynamics in a fluid-solid heterogeneous sphere: a parallel spectral element approximation on non-conforming grids, *J. Comput. Phys.,* **187,** 457–491.

Chamuel, J.R., 1991. Laboratory studies of pulsed leaky Rayleigh wave components in a water layer over a solid bottom, in *Shear Waves in Marine Sediments,* pp. 59–66, eds Hovem, J.M., Richardson, M.D. & Stoll, R.D., Springer.

De Basabe, J.D. & Sen, M.K., 2015. A comparison of finite-difference and spectral-element methods for elastic wave propagation in media with a fluid-solid interface, *Geophys. J. Int.,* **200,** 278–298.

de Hoop, A.T. & van der Hijden, J.H.M.T., 1983. Generation of acoustic waves by an impulsive line source in a fluid/solid configuration with a plane boundary, *J. acoust. Soc. Am.,* **74,** 333–342.

Farnell, G.W., 1970. *Properties of Elastic Surface Waves,* Academic Press.

Glorieux, C., Van de Roystyne, K., Nelson, K.A., Gao, W., Lauriks, W. & Thoen, J., 2001. On the character of acoustic waves at the interface between hard and soft solids and liquids, *J. acoust. Soc. Am.,* **110,** 1299–1306.

Glorieux, C., Van de Roystyne, K., Gusev, V., Gao, W., Lauriks, W. & Thoen, J., 2002. Nonlinearity of acoustic waves at solid-liquid interfaces, *J. acoust. Soc. Am.,* **111,** 95–103.

Komatitsch, D., Barnes, C. & Tromp., J., 2000. Wave propagation near a fluid-solid interface: a spectral element approach, *Geophysics,* **65,** 623–631.

Madec, R., Komatitsch, D. & Diaz, J., 2009. Energy-conserving local time stepping based on high-order finite elements for seismic wave propagation across a fluid-solid interface, *Comput. Model. Eng. Sci.,* **49,** 163–189.

Mittet, R., 2002. Free-surface boundary conditions for elastic staggered-grid modeling schemes, *Geophysics,* **67,** 1616–1623.

Padilla, F., de Billy, M. & Quentin, G., 1999. Theoretical and experimental studies of surface waves on solid-fluid interfaces when the value of the fluid sound velocity is located between the shear and the longitudinal ones in the solid, *J. acoust. Soc. Am.,* **106,** 666–673.

Paillet, F.L. & White, J.E., 1982. Acoustic modes of propagation in the borehole and their relationship to rock properties, *Geophysics,* **47,** 1215–1228.

Phinney, R.A., 1961. Propagation of leaking interface waves, *Bull. seism. Soc. Am.,* **51,** 527–555.

Rauch, D., 1980. Experimental and theoretical studies of seismic interface waves in coastal waters, in *Bottom-Interacting Ocean Acoustics,* pp. 307–327, eds Kupermann, W.A. & Jensen, F.B., Plenum Press.

Scholte, J.G., 1942. On the Stoneley wave equation, *Proc. K. Ned. Akad. Wet.,* **45**(Pt. 1), 20–25, (Pt. 2), 159–164.

Stephen, R.A., 1983. A comparison of finite differences and reflectivity seismograms for marine models, *Geophys. J. R. astr. Soc.,* **22,** 39–58.

Stephen, R.A., 1988. Finite difference methods for bottom interaction problems, in *Computational Acoustics,* pp. 225–238, eds Lee, D., Sternberg, R.L. & Schultz, M.H., North-Holland.

Van Vossen, R., Robertsson, J.O.A. & Chapman, C.H., 2002. Finite-difference modeling of wave propagation in a fluid-solid configuration, *Geophysics,* **67,** 618–624.

Wilcox, L.C., Stadler, G., Burstedde, C. & Ghattas, O., 2010. A high-order discontinuous Galerkin method for wave propagation through coupled elastic-acoustic media, *J. Comput. Phys.,* **229,** 9373–9396.

Zhang, J., 2004. Wave propagation across fluidDsolid interfaces: a grid method approach, *Geophys. J. Int.,* **159,** 240–252.

Zhu, J., Popovics, J.S. & Schubert, F., 2004. Leaky Rayleigh and Scholte waves at the fluid-solid interface subjected to transient point loading, *J. acoust. Soc. Am.,* **116,** 2101–2110.